Structural Characterization of C-Mn Steel Laser Beam Welded Joints with Powder Filler Metal

Weld quality of butt-joint welds with beveled and square edges is investigated

BY S. MISSORI AND A. SILI

ABSTRACT. The possibility of performing successfully sound welds on steel using the laser beam welding (LBW) process with powder filler metal has been used to investigate possible advantages regarding an easier control of the composition of the welded zone. In this work, LBW joints were carried out on C-Mn steel plates with prepared square and beveled edges. Ni filler powder was used as a tracer of the powder penetration inside the joints. The examination of welds included metallographic work by optical and scanning electron microscopy (SEM), with microanalysis by energy-dispersive spectroscopy, to obtain indications on powder distribution. Mechanical properties were evaluated by Vickers microhardness tests.

Introduction

Welding with powder filler metal, using conventional techniques such as arc welding (Ref. 1) and submerged arc welding (Refs. 2–4), could enable enhanced deposition rates. Moreover, the powder addition can offer advantages in the chemical composition of the filler material, particularly where a controlled composition of the welded zone (WZ) is required or when welding materials are not easily combinable. Powder filler metal should allow an improvement of process stability as compared to the risks of incomplete fusion and sticking when using a wire filler material.

In this work, the LBW process has been used to verify the possibility of utilizing powder filler metal. The industrial application of this method could be of interest in the construction of vessels, equipment of large dimensions, ships, etc., thanks to the peculiar characteristics of laser beam welding, *i.e.*, easy automation of the process, reduction of the heat-affected zone and minimizing distortions and residual stresses.

The results of metallurgical investigations on C-Mn steel butt-joint welds, with two different preparations (square and beveled edges) are given. Observations by optical and scanning electron microscopy with microanalysis, by energy dispersive spectroscopy (EDS), were performed to evaluate the depth of powder penetration and the contribution of powder to the formation of a melted pool. The mechanical properties were measured by Vickers microhardness tests.

S. MISSORI is with Department Mechanical Engineering, University of Rome, Tor Vergata, Italy. A. SILI is with Department Industrial, Chemical and Materials Engineering, University of Messina, Italy.

Materials and Methods

Materials

Laser beam welding tests were performed on low-alloy C-Mn steel plates, 10 mm thick, specified as L24N (corresponding to a steel type AISI 15XX with an extra-low content of P and S impurities), having the chemical composition reported in Table 1. The plates were supplied in the normalized condition with a ferritic-pearlitic microstructure.

Commercially pure Ni powder (particle sizes in the range 20–50 μm), transported by an Ar flow, was employed as filler material. The Ni powder was utilized as a tracer because it allows an easy investigation into the distribution of the filler material and the evaluation of the penetration depth along the joint thickness.

KEY WORDS

C-Mn Steel
Powder Filler Metal
Laser Beam Welds (LBW)
Ni Powder Tracing
Welded Zone (WZ)
Heat-Affected Zone (HAZ)

Laser Beam Welding Procedure

The laser system was a continuous CO_2 unit, type TLF12000, with 9 kW of net power on the workpiece. The focusing device was a water-cooled, copper paraboloid mirror. The high power density, focused on a spot of dimension of the order of 0.5 mm, leads to the keyhole mechanism of energy transfer to the workpiece.

A sketch of the process is shown in Fig. 1. The system worked in robotic style with the plates placed in the flat position on a moving table that, translating below the laser head, allows the bead formation in a single pass.

A nozzle with three tubes, arranged as shown in Fig. 1, was utilized for the various gas flows. The welded zone protection was obtained by a primary Ar flow (25 L/min) through tube 3; the powder transportation by a secondary Ar flow (5 L/min) through tube 1; and the plasma control was performed by a He flow (10 L/min) through tube 2.

Many preliminary experiments were performed to optimize the geometric parameters that have a remarkable influence on the powder penetration inside the melted metal (Ref. 5). The nozzle was directed just above the interaction zone of the laser beam and workpiece, in proximity of the melted pool, with an inclination angle of 37 deg. This value was assumed in the middle of the range 30–45 deg in which plasma control and stability can be optimized. Moreover, the powder flow interaction with the workpiece

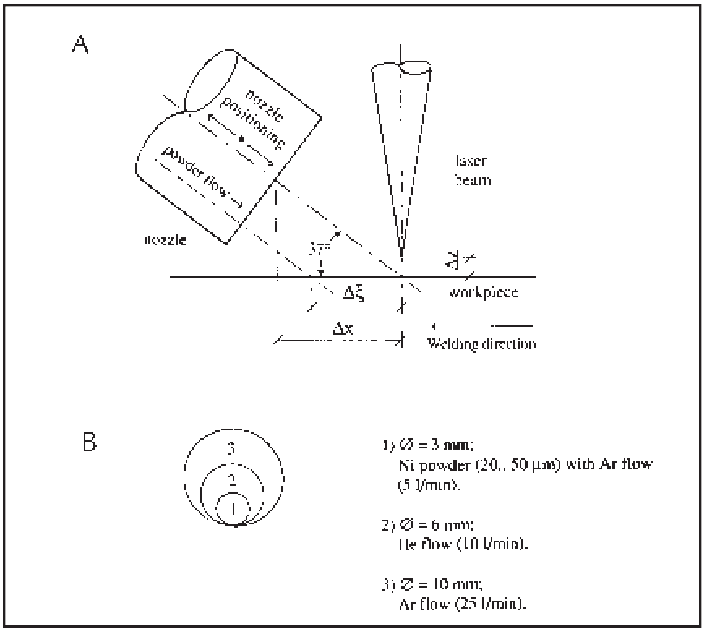

Fig. 1 — A — Sketch of the LBW process; B — nozzle section.

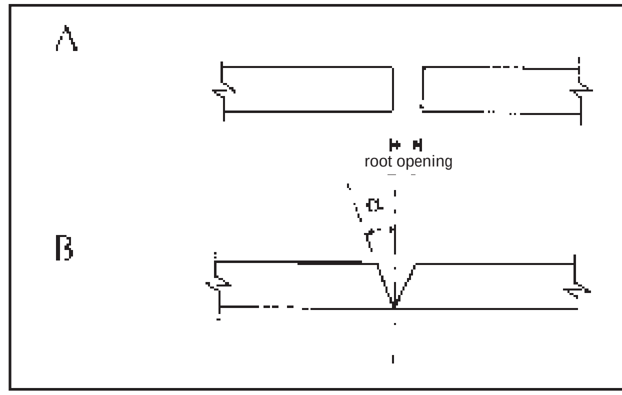

Fig. 2 — Plate preparation of butt-joint welds: A — square edges; B — beveled edges.

and the powder penetration inside the melted pool depend on nozzle and laser beam focus positions. With reference to Fig. 1, the powder trajectory, if approximated by the axis of the smaller tube intersects the workpiece surface at distance ξ from the laser beam axis, has an optimized value equal to 5.8 mm. The distance z between the laser beam focus and workpiece surface has an optimized value equal to 1 mm, and the distance x between the nozzle center and the laser beam axis equal to 8 mm. In any case, according to the process sketched in Fig.1, an adjustment of nozzle positioning can be done by a little translation along its axis that changes the distance x, but keeps constant the distance Δξ between the powder impingement point and the laser beam axis.

Preliminary bead-on-plate tests were permitted to optimize the process parameters, such as the powder rates in the range 20–60 g/min or the welding speed in the range 0.5–1 m/min.

Butt-joint welds were performed on plates with square edges, with a root opening in the range 0–0.4 mm (preparation A), or beveled edge preparation, with bevel angle α = 3, 6, 9 deg and no opening at the root (preparation B), as reported in Fig. 2. The welding speed and powder rate values are given in Table 2.

Experimental Work

The welded plates were cut transversely to the bead to obtain samples of the welded sections. The samples were metallographically prepared by abrasive paper, polished by fine alumina and then etched by 2% Nital.

The following experimental work was performed on the metallographic samples.

A) Visual and macrographic inspections were performed. A minimum number of three macrographic samples per each procedure were cut and examined. The WZ area was measured for each sample.

B) Optical/SEM observations and microanalysis by EDS were performed on metallographic samples taken from each of the welding procedures in order to analyze WZ morphology and assess the Ni content along the thickness of the welds. The Ni content was measured along the centerline of the WZ by an electron probe in a SEM type JSM-35 CF, equipped with an energy-dispersive spectrometer model EDAX 711, at an accelerating voltage of 15 kV. The depth and diameter of the interaction pair were estimated at about 0.5 and 1 μm, respectively. The distance between two microanalysis measurements was equal to about 0.5 mm.

c) Vickers microhardness tests were performed to evaluate the mechanical properties in the welded joints. Measurements were extended to the entire thickness along the centerline of the WZ and to the heat-affected zone (HAZ). Vickers tests were performed with a load of 5 N and a loading time of 10 s.

Results

Visual and Macrographic Inspection

The samples submitted to visual and macrographic inspections confirmed the possibility of having sound welds with a good repeatability (Figs. 3, 4) for both joint preparations. In almost all cases, the penetration was complete along all the plate thickness, and the welds were free from cracks or other defects. However, occasional microcracks in the WZ were revealed. The average values of the WZ area, measured in each sample, are given in Table 3.

Samples welded with square edge preparation show inhomogeneities in the solidification structure, characterized by irregular banding in the WZ — Fig. 3.

Samples welded with beveled edge preparation show the best appearance of the WZ at visual and macrographic examination; the WZ is alloyed enough in Ni to be only weakly etched by Nital — Fig. 4.

Generally, the size and shape of the ferritic steel HAZ is regular and clearly distinct, even if some mismatch (step) of the edges is present, thus demonstrating a good bridgeability of the process. In the macrographs of Figs. 3 and 4, for both joint preparations, the HAZ is clearly observable. The width is gradually varied along the thickness in the range of 1–2 mm, being, in general, larger at the side exposed to the laser beam, corresponding to a wider melted zone.

Microanalysis by EDS

The profiles of Ni concentration along the centerline of the welded sections, which characterize the powder penetration, are reported in Fig. 5 for samples welded with both joint preparations. These diagrams report the best fit of the experimental results and show a Ni penetration along all the weld thickness with a content that, in general, is decreasing along the thickness, starting from the laser beam side. Moreover, the Ni concentration increases when the root opening or the bevel angle values increase.

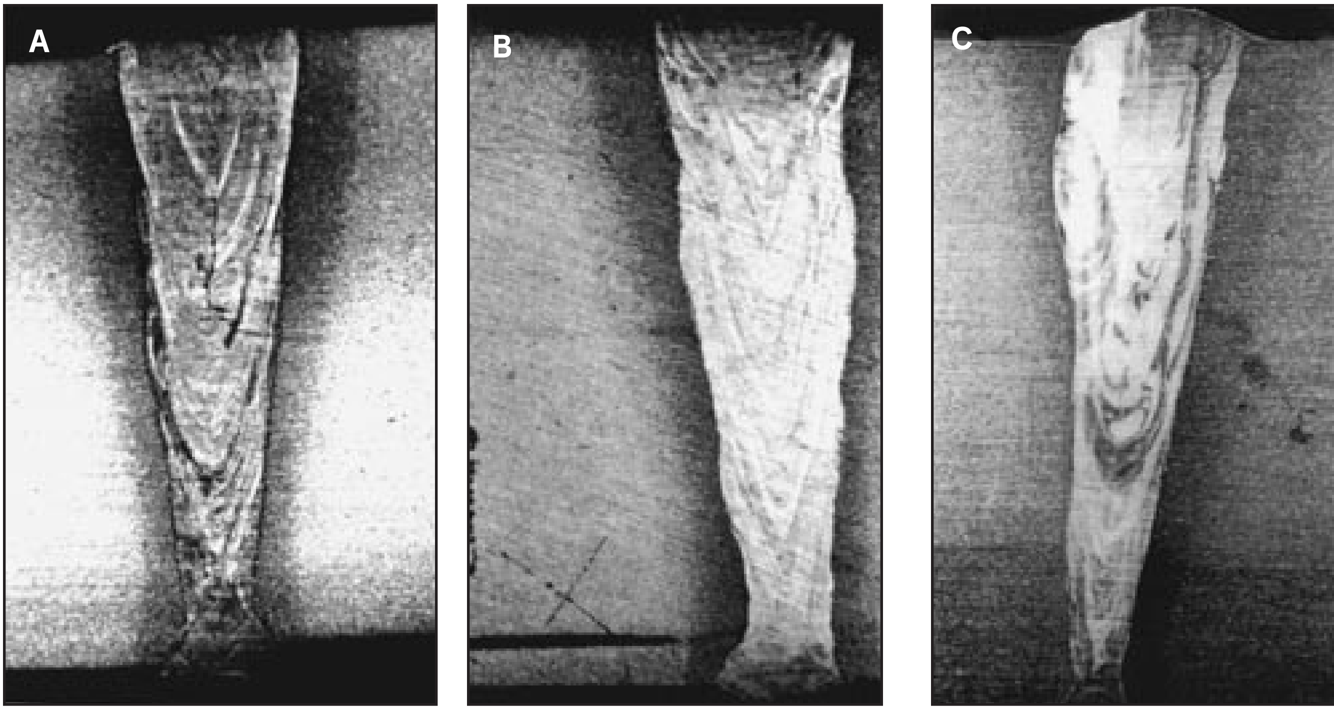

Fig. 3 — Macrograph of welds with square edge preparation: A — root opening = 0; B — root opening = 0.2 mm; C — root opening = 0.4 mm.

Table 1 — Base Material Composition

	C	Si	Mn	P	S	Cr	Ni	Ti	V	Nb	Al
L24N	0.13	—	1.05	0.009	0.002	0.030	0.030	—	—	—	0.041

For samples welded with joint preparation A, the Ni content is in the range 5–3% in weight (0–0.2 mm root opening) and in the range 14–6% in weight (0.4 mm root opening), with higher values at the outer surface (laser beam side).

The most satisfactory results, in terms of powder penetration, are obtained with joint preparation B. In these cases, the Ni content is substantially higher and better distributed along the weld thickness. With a bevel angle of 3 deg, the Ni content profile decreases along the weld thickness from about 22% at the outer surface (laser beam side) to about 10% in weight on the opposite side. With higher bevel angles — 6 and 9 deg — the Ni content is in the range from about 28% at the outer surface (laser beam side) to 20% in weight on the opposite side.

Optical / SEM Observations

A sample with beveled preparation (α = 3 deg) was taken as representative of the metallographic constituents obtained. The metallographic appearance of the WZ at low magnification is shown by the optical micrograph in Fig. 6; details of the solidification structures are

Table 2 — Welding Parameters

Joint preparation	Bevel angle α	Root opening (mm)	Power rate (g/min)	Welding speed (mm/min)
A) square edges		0	20	1000
A) square edges		0.2	20	1000
A) square edges		0.4	35	1000
B) beveled edges	3 deg		40	1000
B) beveled edges	6 deg		60	700
B) beveled edges	9 deg		60	500

Table 3 — Average Values of the WZ Area

Joint preparation	Bevel angle α	Root opening (mm)	WZ area (mm^2)
A) square edges		0	21.2
A) square edges		0.2	21.9
A) square edges		0.4	19.4
B) beveled edges	3 deg		21.4
B) beveled edges	6 deg		28.8
B) beveled edges	9 deg		43.4

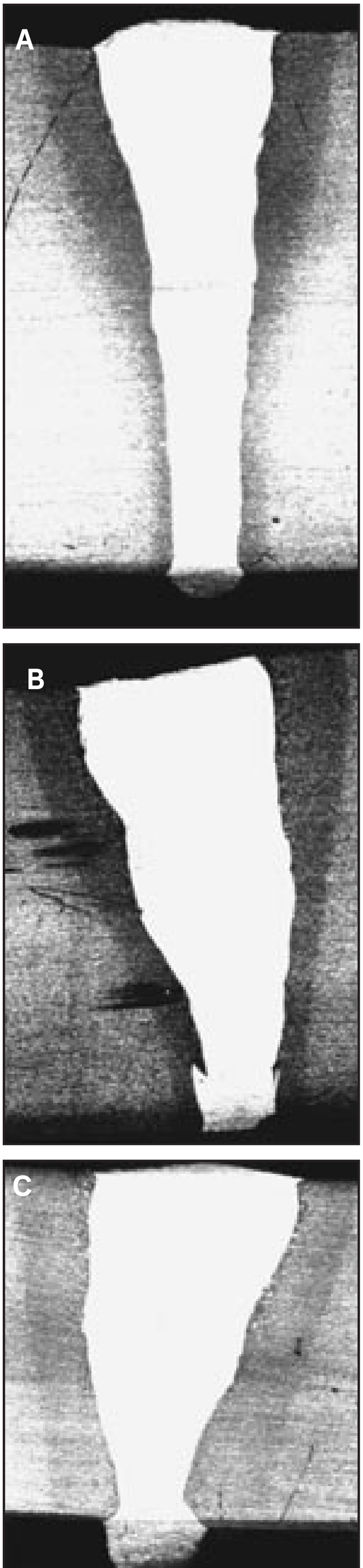

Fig. 4 — Macrograph of welds with beveled edges preparation: A — α = 3 deg; B — α = 6 deg; C — α = 9 deg;

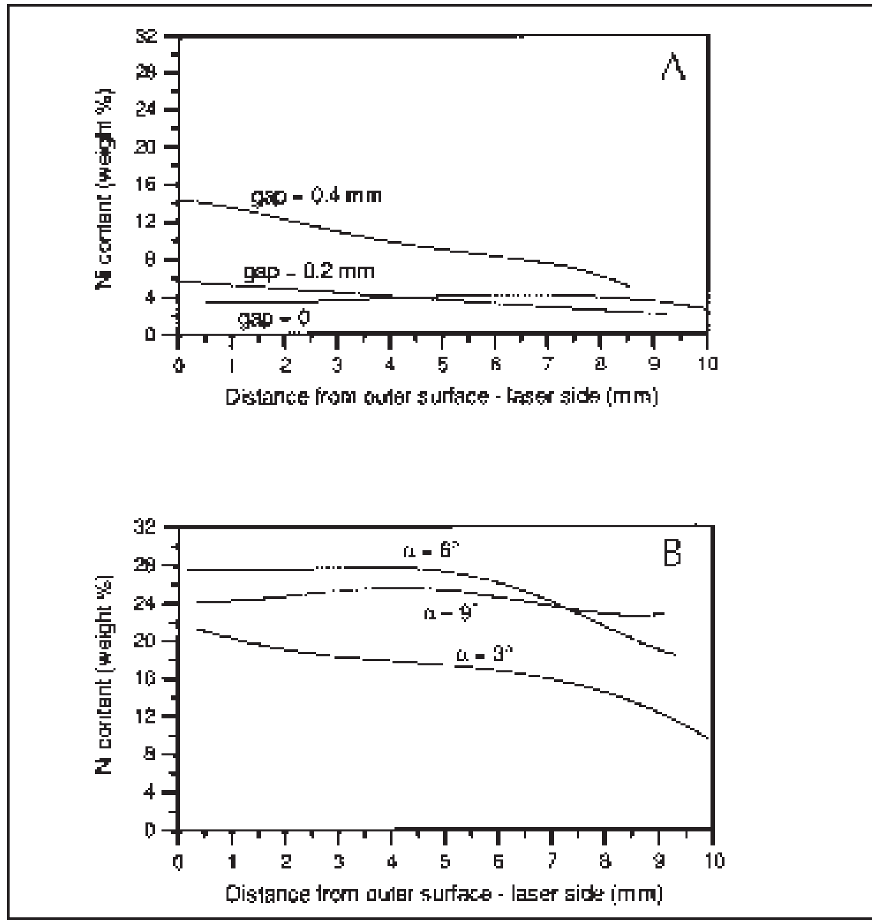

Fig. 5 — Profiles of Ni concentration along the centerline of the welded sections: A — square edge preparation; B — beveled edge preparation.

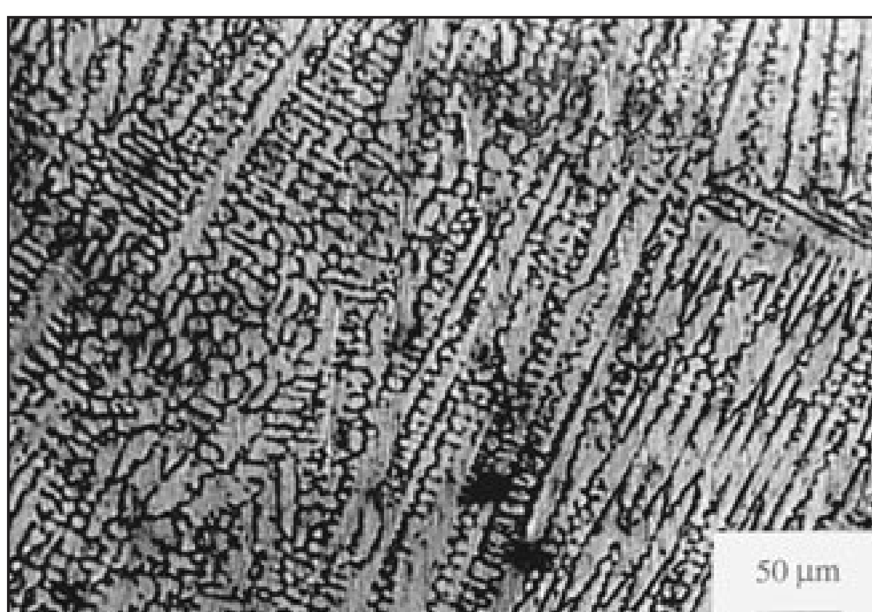

Fig. 6 — Optical micrograph at low magnification of the WZ for a sample with beveled edge preparation and α = 3 deg.

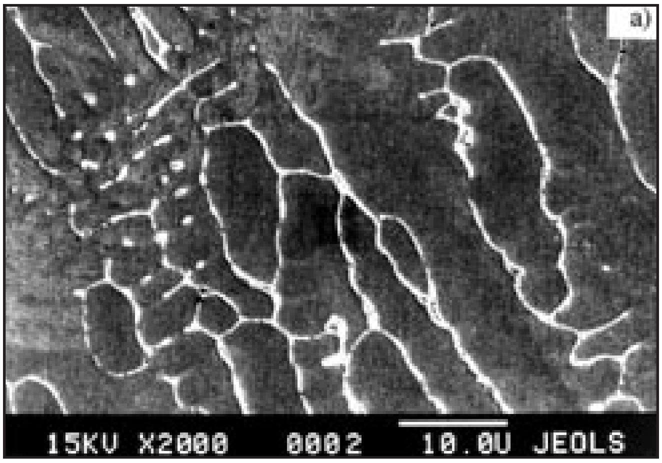

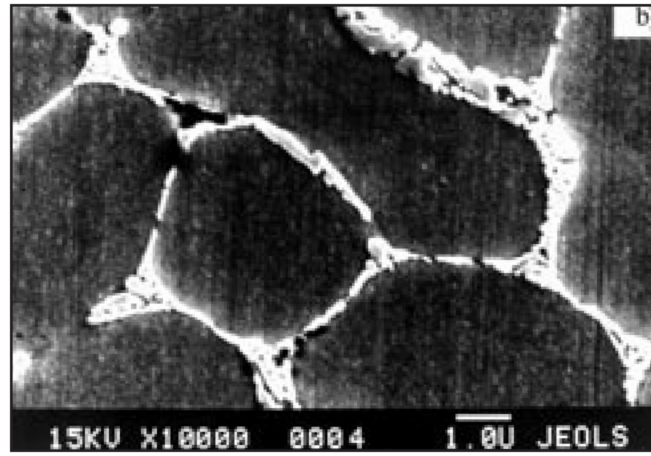

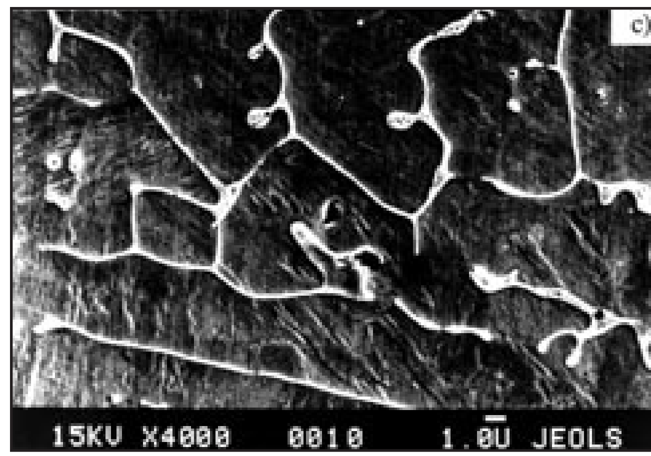

Fig. 7 — SEM images of the WZ for a sample with beveled edge preparation (α = 3 deg): near the outer surface at the laser beam side (a, b); at the opposite side (c).

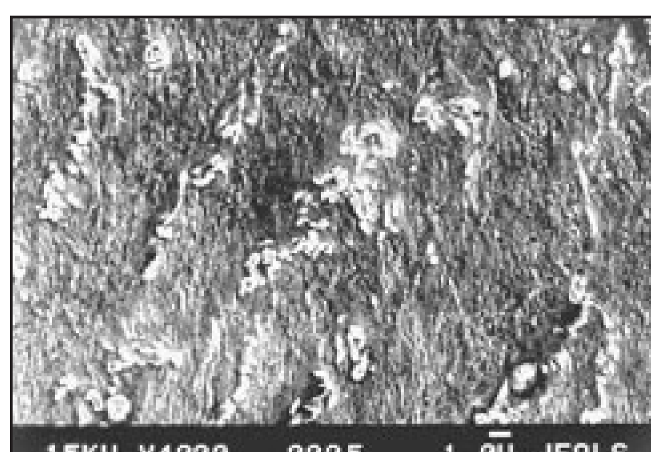

Fig. 8 — SEM images of the WZ for a sample with square edge preparation and root opening = 0.4 mm.

given in the SEM micrographs of Fig. 7. The dendritic solidification structures of the matrix grain are surrounded by an intergranular constituent, whose nature was not identified.

Near the outer surface on the laser beam side (Fig. 7A), the matrix is supposed to be austenitic, according to the high Ni content, which gradually decreases from a value of around 22%, near the outer surface on the laser beam side, to a value of about 10%, on the opposite side — Fig. 5.

Local microanalysis measurements on the intergranular constituent gave a Ni content comparable to the one present in the matrix. On this basis, the interpretation of this constituent as the $FeNi_3$ intermetallic compound has to be excluded. Moreover, in this zone (Fig. 7B) some micropores of dark appearance and rounded elongated shape, having about 1 mm size, are present. These micropores have a morphology similar to that observed in materials produced by powder metallurgy (Ref. 6).

At the opposite side (Fig. 7C), the matrix is characterized by an acicular structure, suggesting the possible presence of martensite, according to the microhardness measurements. Here again, the intergranular constituent surrounding the dendritic matrix grains and some micropores are visible.

The same acicular structure can be observed in the samples welded with the square edge preparation (root opening = 0.4 mm) in the region with the highest values of microhardness — Fig. 8.

Vickers Microhardness Test

For samples welded with joint preparation A, the Vickers microhardness values, measured along the centerline of the welded section, are given in Fig. 9. The hardness fluctuations can be related to solidification structure inhomogeneities, as resulting from the distinct banding revealed by the macrographic inspection — Fig 3. The higher hardness values (above 450 HV) recorded for samples welded with 0.4 mm root openings confirm, on the basis of the Ni content measurements and SEM observations, the presence of martensitic structures.

For joint preparation B with the lower bevel angle (α = 3 deg), the measured values were in the range 200–480 HV — Fig. 10A. The relatively high microhardness values (average value 350 HV) in the zone distant 1–3 mm from the outer surface, laser beam side, are reasonable when taking into account the hardening effects of the high Ni content — Fig. 5. The peak value of 480 HV suggests the presence of martensitic structures, as supported also by the acicular morphology observed in the zone far from the laser beam side — Fig. 7C.

With the other values of bevel angle

Table 4 — Expected and Experimental Average Ni Content

Joint preparation	Bevel angle α	Root opening (mm)	Expected Ni content (wt-%)	Average Experimental Ni content (wt-%)
A) square edges		0	11	4
A) square edges		0.2	11	4
A) square edges		0.4	22	10
B) beveled edges	3 deg		23	17
B) beveled edges	6 deg		36	25
B) beveled edges	9 deg		34	24

(α = 6 and 9 deg), the hardness profiles along the centerline of the welded sections are characterized by values around 200 HV and by the absence of relevant fluctuations — Fig. 10. Considering the high Ni content (a range of 20–28% in weight) recorded by microanalysis measurements, these low hardness values can be ascribed to austenitic structures, which are present along all the weld thickness.

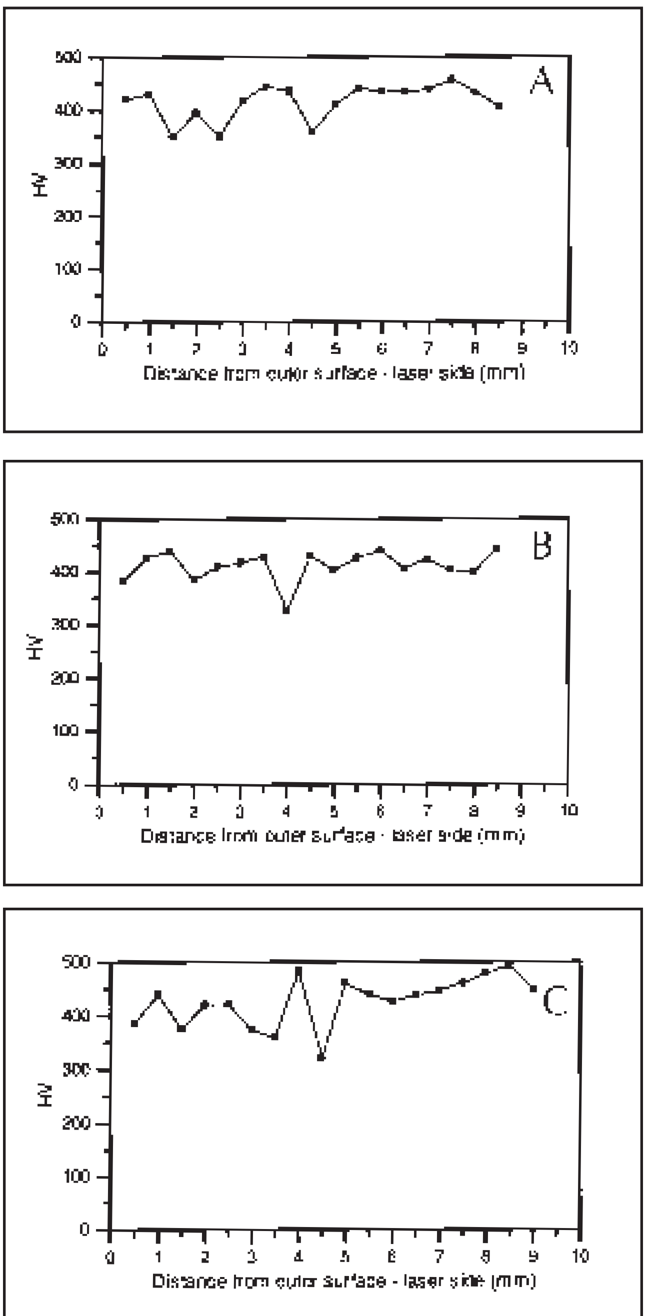

Fig. 9 — Vickers microhardness profiles along the centerline of the welded sections for samples with square edges preparation: A — root opening = 0; B — root opening = 0.2 mm; C — root opening = 0.4 mm.

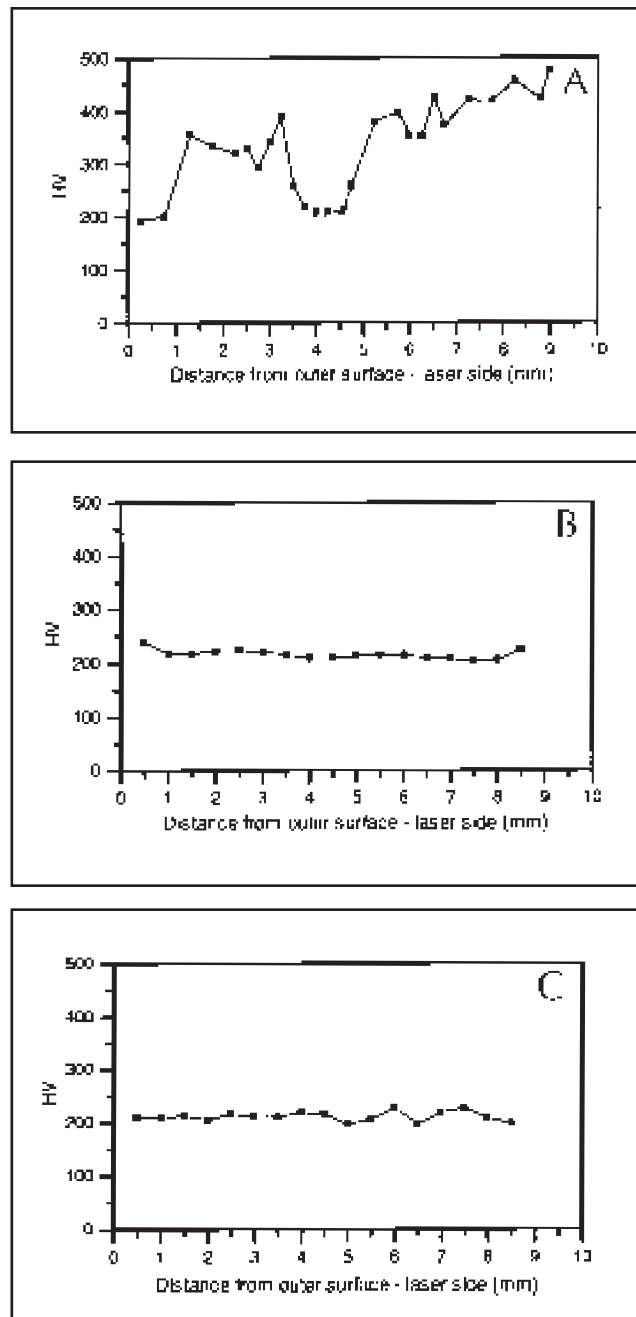

Fig. 10 — Vickers microhardness profiles along the centerline of the welded sections for samples with beveled edges preparation: A — α = 3 deg; B — α = 6 deg; C — α = 9 deg.

Discussion

In order to estimate which is the best geometry to convey the powder flow into the melted pool, the expected Ni content, calculated on the basis of the welding parameters and of the measured WZ area, was compared with the Ni content along the welded sections experimentally obtained by microanalysis.

As a result of microanalysis measurements, the contribution to the joint formation is given by the base metal, with density δ_{Fe}=7.87 10^{-3} g/mm^3 and concentration C_{Fe} (weight fraction), and by the Ni powder, with density δ_{Ni}=8.9 10^{-3} g/mm^3 and concentration C_{Ni} (weight fraction). So, for a welded volume having as base the WZ area A_S (mm^2) and a height of 1 mm, considering the powder rate p (g/min) and the welding speed v_S (mm/min), the expected Ni content is given by the following expression:

$$C_{Ni} = p / [(\delta_{Ni} C_{Ni} + \delta_{Fe} C_{Fe}) \times v_S \times A_S] \qquad (1)$$

The average value of the Ni content experimental profile along the welded section, obtained by microanalysis measurements, was considered representative of the Ni content along the welded sections.

In Table 4, expected and experimental average Ni content are compared for both joint preparations. The experimental average values are, in any case, lower than the expected ones, due to probable powder loss. From data reported in Table 4, the ratio of the experimental average Ni content to the expected Ni content results are about 0.4 for joint preparation A and about 0.7 for joint preparation B. So, the best results appear to be those obtained in the samples welded with a beveled joint, in which the experimental average Ni content shows the best approximation to the expected one.

With the beveled joint preparation, the powder conveyed by the gas flow is “funneled” and forced to melt into the space between the edges. On the contrary, when welding using square edges with little or no root opening, the possibility of the powder penetrating between the edges is drastically reduced and part of the filler powder is blown away with the process gas.

Generally, samples butt-joint welded with square edges gave rise to a low contribution of the powder filler metal to the formation of the WZ, revealed by the lean content of nickel and, occasionally, with presence of cracks observed on macrographs and micrographs.

In some welded sections of joints with beveled edge preparation, the presence of rounded and elongated micropores (representative size of 1 mm) were observed. These micropores are similar to those often found in materials produced by powder metallurgy.

Conclusions

The experimental work contributed to the setup of the laser beam welding process with a single pass by utilization of filler metal powder. The obtainable distribution of the filler metal and its alloy elements along the thickness of butt-joint welds was considered for two different preparations — square and beveled edges.

- The powder penetration along the weld thickness decreased starting from the outer surface at the laser beam side.
- For square edge preparation, the Ni content increased at the increasing of the root opening between plate edges, but it is always very low in respect to the expected value.
- The highest contribution of the filler powder to the formation of the weld zone was obtained with the beveled joint preparation, reaching about 70% of the Ni expected content.
- In some welded sections, particularly those for joints with beveled edge preparation, the presence of rounded and elongated micropores, similar to those often found in materials produced by powder metallurgy, were observed.

Acknowledgments

This work was supported by the Human Capital and Mobility Program of the European Community within the framework of the project European Laser Center at the Fraunhofer Institut für Lasertechnik in Aachen, Germany. The author wishes to thank Dipl. Ing. W. Frohn of the Laser Welding Department of ILT-Aachen for his extensive support in setting up welding procedures and technical assistance. Grateful thanks are due to the management of ILT.

References

1. Campbell, C., and Johnson, W. C. 1967. Granular metal filler metals for arc welding. *Welding Journal* 46(3): 200–208.
2. Troyer, W., and Mikurak, J. 1974. High deposition submerged arc welding with iron powder joint fill. *Welding Journal* 53(8): 494–300.
3. Rodgers, J., and Lochhead, J. C. 1987. Submerged arc welding with metal powder additions, productivity and properties. *Welding Journal* 66(10): 21–27.
4. Bailey, N. 1991. Submerged arc welding ferritic steels with alloyed metal powder. *Welding Journal* 70(8): 187–194.
5. Sili, A. 1998. Laser beam welding of HSLA steels with utilization of powder filler metal. CEC Project — Final report, User Selection Panel Meeting. Fraunhofer Institut für Lasertechnik—ILT, Aachen, Germany.
6. Metallography and Microstructures. 1985. *Metals Handbook,* Ninth Ed., Vol. 9. ASM, Materials Park, Ohio, p. 504–530.